Available online at www.sciencedirect.com

ScienceDirect

Journal of Sound and Vibration 315 (2008) 212–225

JOURNAL OF SOUND AND VIBRATION

www.elsevier.com/locate/jsvi

A hybrid layerwise and differential quadrature method for in-plane free vibration of laminated thick circular arches

P. Malekzadeh[a,b,*], A.R. Setoodeh[c], E. Barmshouri[d]

[a]Department of Mechanical Engineering, Persian Gulf University, Boushehr 75168, Iran
[b]Center of Excellence for Computational Mechanics in Mechanical Engineering, Shiraz University, Shiraz, Iran
[c]Department of Mechanical Engineering, Faculty of Engineering, Ferdowsi University of Mashhad, Mashhad 91775, Iran
[d]Department of Civil Engineering, Persian Gulf University, Boushehr 75168, Iran

Received 23 April 2007; received in revised form 6 February 2008; accepted 7 February 2008
Handling Editor: C. Morfey
Available online 14 March 2008

Abstract

An accurate and efficient solution procedure based on the two-dimensional elasticity theory for free vibration of arbitrary laminated thick circular deep arches with some combinations of classical boundary conditions is introduced. In order to accurately represent the variation of strain across the thickness, the layerwise theory is used to approximate the displacement components in the radial direction. Employing Hamilton's principle, the discretized form of the equations of motion and the related boundary conditions in the radial direction are obtained. The resulting governing equations are then discretized using the differential quadrature method (DQM). After performing the convergence studies, new results for laminated arches with different set of boundary conditions are developed. Additionally, different values of the arch parameters such as opening angle, thickness-to-length and orthotropy ratios are considered. In all cases, comparisons with the results obtained using the finite element software 'ABAQUS' and also with those of the first- and higher-order shear deformation theories available in the literature are performed. Close agreements, especially with those of ABAQUS, are achieved.

1. Introduction

Laminated composite circular arches have found wide applications as structural members in aerospace, marine and other industries. In comparison with research works on the free vibration analyses of isotropic arches, some of which can be found in Refs. [1–3], only limited references can be found on laminated composite arches [4–11].

Transverse shear deformation and rotary inertia have significant effects on the natural frequencies of the thick composite arches, especially on the higher-order modes. Most of the previous works are based on the

*Corresponding author at: Department of Mechanical Engineering, Persian Gulf University, Boushehr 75168, Iran.
Tel.: +98 771 4222150; fax: +98 771 4540376.
E-mail addresses: malekzadeh@pgu.ac.ir, p_malekz@yahoo.com (P. Malekzadeh).

0022-460X/$ - see front matter
doi:10.1016/j.jsv.2008.02.005

Nomenclature

A_{mn}^{ij}	stiffness coefficient
A_{ij}^{θ}	first-order DQ weighting coefficients
b	width of the arch
B_{mn}^{ij}	stiffness coefficient
B_{ij}^{θ}	second-order DQ weighting coefficients
$\mathbf{C}$	two-dimensional material stiffness matrix
C_{ij}	two-dimensional material stiffness
$\mathbf{C}'$	three-dimensional material stiffness matrix
$\overline{\mathbf{C}}$	three-dimensional material stiffness matrix in principal material coordinates
D	amplitude of domain degrees of freedom
D_{mn}^{ij}	stiffness coefficient
h	total thickness of the arch
I^{ij}	inertia coefficients
$F_{r\theta}^{i}$	generalized transverse shear forces
$\mathbf{K}_{bb}$	boundary stiffness matrices
$\mathbf{K}_{bd}$	boundary stiffness matrices
$\mathbf{K}_{db}$	domain stiffness matrices
$\mathbf{K}_{dd}$	domain stiffness matrices
$\mathbf{M}$	mass matrix
n_e	number of elements in ABAQUS modeling
n_L	number of orthotropic layers
n_m	number of mathematical layers through the thickness of the arch
n_r	total number of nodes through the thickness of the arch
n_θ	number of DQ grid points
$N_{\theta\theta}^{i}$	generalized axial forces
r	radial coordinate variable
r_i	radial position of node i
R	mean radius of the arch
R_i	inner radius of the arch
R_o	outer radius of the arch
t	time
$\mathbf{T}$	transformation matrix
U_i	nodal values of the displacement components u
V_i	nodal values of the displacement components v
W_{ij}^{m}	mth-order DQ weighting coefficients
θ	tangential coordinate variable
θ_0	opening angle of the arch
φ_i	global Lagrange interpolation functions in the r-direction
ω_i	ith natural frequencies
ϖ_i	ith non-dimensional natural frequencies $[=\omega_i(L^2/h)\sqrt{12\rho/E_1}]$
$\gamma_{r\theta}$	transverse shear strain component
$\boldsymbol{\varepsilon}$	vector of strain components
$\boldsymbol{\varepsilon}_i$	vector of in-plane strain components
$\boldsymbol{\varepsilon}_o$	vector of out-of-plane strain components
ε_{rr}	normal strain component in the r-direction
$\varepsilon_{\theta\theta}$	normal strain component in the θ-direction
$\boldsymbol{\sigma}_i$	vector of in-plane stress components
$\boldsymbol{\sigma}_o$	vector of out-of-plane stress components
σ_{rr}	normal stress component in the r-direction
$\sigma_{r\theta}$	transverse shear stress component
$\sigma_{\theta\theta}$	normal stress component in the θ-direction
$(\ )^{-1}$	inverse of matrix ( )

one-dimensional single-layer theories such as the classical theory [5,6], the first and higher-order shear deformation theories [4,7–11]. The classical laminate theory neglects the shear deformation and rotary inertia effects.

Exact solutions can be obtained straightforwardly for thin and thick arches with simply supported boundary conditions. To study the free vibration of laminated composite arches with general boundary conditions, usually numerical approximate methods such as the finite element and Ritz methods [4–6,9] are used.

The layerwise theory is a refined theory that can take into account the thickness effects with minimum computational cost [12–15]. Unlike the equivalent single-layer theories [4–11], the layerwise theories assume separate displacement field expansions within each subdivision. Hence, the layerwise theory provides a kinematically correct representation of the strain field in discrete layers [12–16]. This is an advantage of the layerwise theories in comparison with higher-order shear deformation theories. Since the shear strains are discontinuous, this leaves the possibility of the continuous transverse stresses between adjacent layers in the layerwise theory.

Differential quadrature method (DQM) as an alternative numerical technique was used for the solution of structural problems. The development and its recent applications can be found in a review paper by Bert and Malik [16] and also in the research works of Malekzadeh and his co-workers [17–21]. To the authors' best knowledge, a mixed application of DQ and layerwise theory for composite structures has not yet been reported.

Due to the through-the-thickness material discontinuity, the conventional DQM cannot be used for the two-dimensional elasticity analysis of laminated composite arches problems. Hence, in this paper, using the two-dimensional layerwise theory in conjunction with the DQ method, a hybrid numerical method is introduced for the in-plane free vibration analysis of thick laminated deep arches with some combinations of classical boundary conditions (simply supported, clamped and free) and general boundary conditions. The convergence behaviors of the method against the number of mathematical layers and DQ grid points are investigated. Comparisons with the results of the first-order shear deformation theory (FSDT), the higher-order shear deformation theory (HSDT) and in all cases with finite element based software ABAQUS [22] are made. Considering the effects of different parameters such as opening angle, thickness-to-length and orthotropy ratios, some new results for the natural frequencies of the laminated arches are developed.

2. Basic relations

Consider a laminated thick circular deep arch composed of n_L perfectly bonded orthotropic layers of width b, total thickness h, opening angle θ_0 and mean radius R (Fig. 1). Based on the two-dimensional theory of elasticity, the linearized in-plane strain–displacement relations are as follows:

$$\boldsymbol{\varepsilon}_i^{\mathrm{T}} = [\varepsilon_{\theta\theta}, \quad \varepsilon_{rr}, \quad \gamma_{r\theta}] = \left[\frac{1}{r}\left(u + \frac{\partial v}{\partial \theta}\right), \quad \frac{\partial u}{\partial r}, \quad \frac{1}{r}\left(\frac{\partial u}{\partial \theta} - v\right) + \frac{\partial v}{\partial r}\right]. \tag{1}$$

In the equivalent single-layer theories of beams, in addition to the assumptions of plane stress or strain in the width direction, the normal stress in the thickness direction (σ_{rr}) was neglected to express the stress–strain relations for each layer. But, here, this assumption is removed. However, since the width of the arch is supposed to be small in comparison with the thickness, the plane stress assumption is employed, i.e. $\sigma_{zr} = \sigma_{z\theta} = \sigma_{zz} = 0$. To derive the stress–strain relations at an arbitrary point of a laminae, the

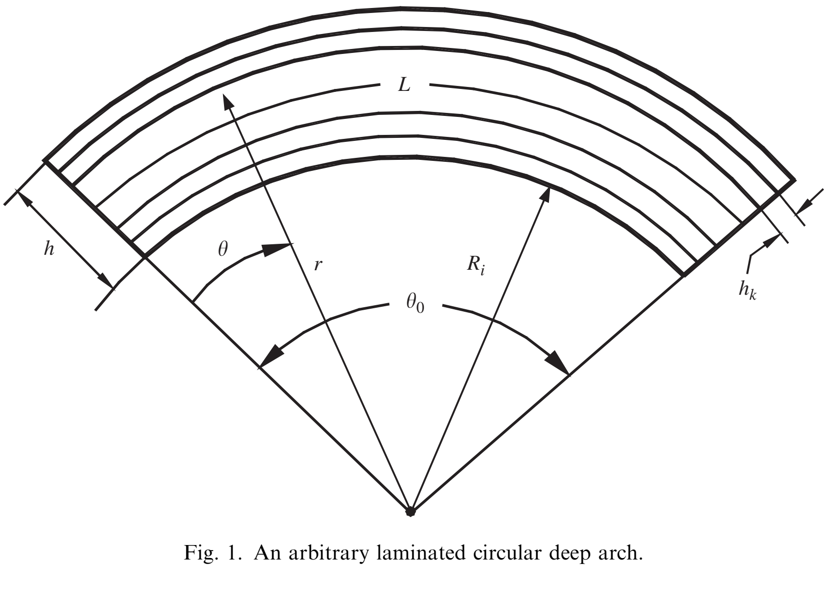

Fig. 1. An arbitrary laminated circular deep arch.

three-dimensional constitutive relations is used, which is

$$\begin{Bmatrix} \sigma_{\theta\theta} \\ \sigma_{rr} \\ \sigma_{zz} \\ \sigma_{r\theta} \\ \sigma_{rz} \\ \sigma_{z\theta} \end{Bmatrix} = \begin{bmatrix} C'_{11} & C'_{12} & C'_{13} & 0 & 0 & C'_{16} \\ C'_{12} & C'_{22} & C'_{23} & 0 & 0 & C'_{26} \\ C'_{13} & C'_{23} & C'_{33} & 0 & 0 & C'_{36} \\ 0 & 0 & 0 & C'_{44} & C'_{45} & 0 \\ 0 & 0 & 0 & C'_{45} & C'_{55} & 0 \\ C'_{16} & C'_{26} & C'_{36} & 0 & 0 & C'_{66} \end{bmatrix} \begin{Bmatrix} \varepsilon_{\theta\theta} \\ \varepsilon_{rr} \\ \varepsilon_{zz} \\ \gamma_{r\theta} \\ \gamma_{rz} \\ \gamma_{z\theta} \end{Bmatrix} = \mathbf{C}'\boldsymbol{\varepsilon}, \tag{2}$$

where $\mathbf{C}' = \mathbf{T}\overline{\mathbf{C}}\mathbf{T}^{\mathrm{T}}$; $\overline{\mathbf{C}}$ is the material stiffness matrix in the material principal coordinates of the laminae and $\mathbf{T}$ represents the transformation matrix [13].

In order to implement the plane stress conditions, Eq. (2) can be rearranged as

$$\begin{Bmatrix} \boldsymbol{\sigma}_i \\ \boldsymbol{\sigma}_o \end{Bmatrix} = \begin{bmatrix} \mathbf{C}^{ii} & \mathbf{C}^{io} \\ \mathbf{C}^{oi} & \mathbf{C}^{oo} \end{bmatrix} \begin{Bmatrix} \boldsymbol{\varepsilon}_i \\ \boldsymbol{\varepsilon}_o \end{Bmatrix}, \tag{3}$$

where

$$\boldsymbol{\sigma}_i = \begin{Bmatrix} \sigma_{\theta\theta} \\ \sigma_{rr} \\ \sigma_{r\theta} \end{Bmatrix}, \quad \boldsymbol{\sigma}_o = \begin{Bmatrix} \sigma_{zz} \\ \sigma_{rz} \\ \sigma_{z\theta} \end{Bmatrix}, \quad \boldsymbol{\varepsilon}_o = \begin{Bmatrix} \varepsilon_{zz} \\ \gamma_{rz} \\ \gamma_{z\theta} \end{Bmatrix} \quad \text{and} \quad \mathbf{C}^{ii} = \begin{bmatrix} C'_{11} & C'_{12} & 0 \\ C'_{12} & C'_{22} & 0 \\ 0 & 0 & C'_{44} \end{bmatrix},$$

$$\mathbf{C}^{io} = \begin{bmatrix} C'_{13} & 0 & C'_{16} \\ C'_{23} & 0 & C'_{26} \\ 0 & C'_{45} & 0 \end{bmatrix}, \quad \mathbf{C}^{oi} = \begin{bmatrix} C'_{13} & C'_{23} & 0 \\ 0 & 0 & C'_{45} \\ C'_{16} & C'_{26} & 0 \end{bmatrix}, \quad \mathbf{C}^{oo} = \begin{bmatrix} C'_{33} & 0 & C'_{36} \\ 0 & C'_{55} & 0 \\ C'_{36} & 0 & 0 \end{bmatrix}.$$

Using the conditions of zero stress vector on the z-plane, i.e. $\boldsymbol{\sigma}_o = 0$, one obtains

$$\boldsymbol{\sigma}_i = \mathbf{C}\,\boldsymbol{\varepsilon}_i, \tag{4}$$

where $\mathbf{C} = \mathbf{C}^{ii} - \mathbf{C}^{io}(\mathbf{C}^{oo})^{-1}\mathbf{C}^{oi}$.

3. Equations of motion and boundary conditions

To develop a layerwise model for the arches that posses full two-dimensional modeling capability, either for state of plane stress or strain, a displacement field that accounts for all the three strain components in a kinematically correct manner must be assumed. Specifically, the in-plane strain $\varepsilon_{\theta\theta}$ should be continuous while the transverse strain $\gamma_{r\theta}$ should be piecewise continuous through the laminate thickness.

In order to build a high degree of transverse discretization generality into the model, the layerwise laminate theory of Reddy [13] is used to introduce the following expansions for the displacement components:

$$u_r = u(r,\theta,t) = \sum_{i=1}^{n_r} U_i(\theta,t)\varphi_i(r) = U_i(\theta,t)\varphi_i(r), \quad u_\theta = v(r,\theta,t) = V_i(\theta,t)\varphi_i(r), \tag{5}$$

where as obvious from Eq. (5), for brevity purpose, the indicial summation rule is used henceforth. φ_i denotes the global interpolation function in the r-direction. Also U_i and V_i represent the displacement components of all points located on the ith plane (defined by $r = r_i$) in the r- and θ-directions, respectively. Additionally, n_r stands for the total number of nodes through the thickness of the arch, which depends on the number of mathematical layers (n_m) and nodes per layer in the thickness direction.

In the present study, one-dimensional Lagrange interpolation functions are used in each mathematical layer and hence the global interpolation function $\varphi_i(r)$ can easily be obtained. The layerwise concept is general such that the number of subdivisions can be greater than, equal to, or less than the number of material layers through the thickness. Any desired degree of displacement variation through the thickness are easily obtained by either adding more subdivisions (mathematical layers) or using higher-order Lagrangian interpolation polynomials through the thickness.

Substituting the displacement components from Eq. (5) into Eq. (1), the results read

$$\varepsilon_{rr} = U_i(\theta,t)\frac{\mathrm{d}\varphi_i(r)}{\mathrm{d}r}, \quad \varepsilon_{\theta\theta} = \frac{\varphi_i(r)}{r}\left[U_i(\theta,t) + \frac{\partial V_i(\theta,t)}{\partial\theta}\right], \quad \gamma_{r\theta} = \frac{\varphi_i(r)}{r}\left[\frac{\partial U_i(\theta,t)}{\partial\theta} - V_i(\theta,t)\right] + V_i(\theta,t)\frac{\mathrm{d}\varphi_i(r)}{\mathrm{d}r}. \tag{6}$$

The equations of motion at each node can be obtained by using Hamilton's principle, which, in this case turns into

$$\int_{t_1}^{t_2}(\delta U - \delta T)\,\mathrm{d}t = \int_{t_1}^{t_2}\left\{\int_0^{\theta_0}\int_{R_i}^{R_o}[\sigma_{rr}\delta\varepsilon_{rr} + \sigma_{\theta\theta}\delta\varepsilon_{\theta\theta} + \sigma_{r\theta}\delta\gamma_{r\theta} - \rho(\dot{u}\delta\dot{u} + \dot{v}\delta\dot{v})]br\,\mathrm{d}r\,\mathrm{d}\theta\right\}\mathrm{d}t = 0. \tag{7}$$

Insertion of Eqs. (4) and (6) into Eq. (7), followed by integration with respect to the thickness coordinate r and also integration by parts with respect to coordinate θ and time t, yields the equations of motion and the related boundary conditions at each node i with $i = 1,2,\ldots,n_r$ as follows:*Equations of motion*:

δU_i:

$$\begin{aligned}&-A_{33}^{ij}\frac{\partial^2 U_j}{\partial\theta^2} + (B_{23}^{ij} - B_{23}^{ji})\frac{\partial U_j}{\partial\theta} + (A_{11}^{ij} + B_{12}^{ji} + B_{12}^{ij} + D_{22}^{ij})U_j - A_{13}^{ij}\frac{\partial^2 V_j}{\partial\theta^2}\\ &+ (A_{11}^{ij} + A_{33}^{ij} - B_{33}^{ji} + B_{12}^{ij})\frac{\partial V_j}{\partial\theta} - (A_{13}^{ij} - B_{13}^{ji} + B_{23}^{ij} - D_{23}^{ij})V_j + I^{ij}\ddot{U}_j = 0,\end{aligned} \tag{8}$$

δV_i:

$$\begin{aligned}&-A_{13}^{ij}\frac{\partial^2 U_j}{\partial\theta^2} - (A_{11}^{ij} + A_{33}^{ij} + B_{12}^{ji} - B_{33}^{ij})\frac{\partial U_j}{\partial\theta} - (A_{13}^{ij} - B_{13}^{ij} + B_{23}^{ji} - D_{23}^{ij})U_j\\ &- A_{11}^{ij}\frac{\partial^2 V_j}{\partial\theta^2} + (B_{13}^{ij} - B_{13}^{ji})\frac{\partial V_j}{\partial\theta} + (A_{33}^{ij} - B_{33}^{ji} - B_{33}^{ij} + D_{33}^{ij})V_j + I^{ij}\ddot{V}_j = 0.\end{aligned} \tag{9}$$

Boundary conditions:

$$\text{Either } U_i = 0 \text{ or } F_{r\theta}^i = A_{33}^{ij}\frac{\partial U_j}{\partial\theta} + (A_{13}^{ij} + B_{23}^{ji})U_j + A_{13}^{ij}\frac{\partial V_j}{\partial\theta} - (A_{33}^{ij} + B_{33}^{ji})V_j = 0, \tag{10}$$

$$\text{Either } V_i = 0 \text{ or } N_{\theta\theta}^i = A_{13}^{ij}\frac{\partial U_j}{\partial\theta} + (A_{11}^{ij} + B_{12}^{ji})U_j + A_{11}^{ij}\frac{\partial V_j}{\partial\theta} - (A_{13}^{ij} - B_{13}^{ji})V_j = 0, \tag{11}$$

where $F_{r\theta}^i$ and $N_{\theta\theta}^i$ are the generalized shear and axial forces, respectively. In the above equations, unlike the first approximation type, the stiffness and inertia coefficients are obtained by exact integrations from the following expressions:

$$\begin{aligned}A_{mn}^{ij} &= \int_{R_i}^{R_o} bC_{mn}\left(\frac{\varphi_i\varphi_j}{r}\right)\mathrm{d}r, \quad B_{mn}^{ij} = \int_{R_i}^{R_o} bC_{mn}\varphi_j\frac{\mathrm{d}\varphi_i}{\mathrm{d}r}\,\mathrm{d}r,\\ D_{mn}^{ij} &= \int_{R_i}^{R_o} bC_{mn}\frac{\mathrm{d}\varphi_i}{\mathrm{d}r}\frac{\mathrm{d}\varphi_j}{\mathrm{d}r}r\,\mathrm{d}r, \quad I^{ij} = \int_{R_i}^{R_o} b\rho\varphi_i\varphi_j r\,\mathrm{d}r.\end{aligned} \tag{12}$$

It is obvious that the approximate numerical methods such as finite element method (FEM), finite difference or differential quadrature method [3,16–21] can easily be used to solve the resulting layerwise equations of motion subjected to the related boundary conditions. Due to high accuracy of the DQM and its low computational efforts, this method is employed in this study.

4. DQ discretization

In order to use the DQ method to discretize the governing equations in the axial direction θ, each mathematical layer is discretized into a set of n_θ grid points in this direction. Then, at each boundary or domain grid points, the spatial derivatives are discretized according to the DQ-rules for derivatives. A brief review of the DQM is presented in Appendix A. Using the DQ discretization rules, for an arbitrary layer i and at each domain grid point k with $k = 2,3,\ldots,n_\theta-1$, the equations of motion (1–3) become

Eq. (8):

$$-A_{33}^{ij}\sum_{m=1}^{n_\theta} W_{km}^2 U_{mj} + (B_{23}^{ij} - B_{23}^{ji})\sum_{m=1}^{n_\theta} W_{km}^1 U_{mj} + (A_{11}^{ij} + B_{12}^{ji} + B_{12}^{ij} + D_{22}^{ij})U_{kj} - A_{13}^{ij}\sum_{m=1}^{n_\theta} W_{km}^2 V_{mj}$$
$$+ (A_{11}^{ij} + A_{33}^{ij} - B_{33}^{ji} + B_{12}^{ij})\sum_{m=1}^{n_\theta} W_{km}^1 V_{mj} - (A_{13}^{ij} - B_{13}^{ji} + B_{23}^{ij} - D_{23}^{ij})V_{kj} + I^{ij}\ddot{U}_{kj} = 0. \tag{13}$$

Eq. (9):

$$-A_{13}^{ij}\sum_{m=1}^{n_\theta} W_{km}^2 U_{mj} - (A_{11}^{ij} + A_{33}^{ij} + B_{12}^{ji} - B_{33}^{ij})\sum_{m=1}^{n_\theta} W_{km}^1 U_{mj} - (A_{13}^{ij} - B_{13}^{ij} + B_{23}^{ji} - D_{23}^{ij})U_j$$
$$- A_{11}^{ij}\sum_{m=1}^{n_\theta} W_{km}^2 V_{mj} + (B_{13}^{ij} - B_{13}^{ji})\sum_{m=1}^{n_\theta} W_{km}^1 V_{mj} + (A_{33}^{ij} - B_{33}^{ji} - B_{33}^{ij} + D_{33}^{ij})V_{kj} + I^{ij}\ddot{V}_{kj} = 0. \tag{14}$$

Hereafter f_{ij} stands for $f(r_i,\theta_j,t)$. In a similar manner the DQ analogs of the boundary conditions for the ith layer can be obtained:

Eq. (10):

$$\text{Either } U_{k_i} = 0 \text{ or } F_{r\theta}^{ki} = A_{33}^{ij}\sum_{m=1}^{n_\theta} W_{km}^1 U_{mj} + (A_{13}^{ij} + B_{23}^{ji})U_{kj}$$
$$+ A_{13}^{ij}\sum_{m=1}^{n_\theta} W_{km}^1 V_{mj} - (A_{33}^{ij} + B_{33}^{ji})V_{kj} = 0. \tag{15}$$

Eq. (11):

$$\text{Either } V_{k_i} = 0 \text{ or } N_{\theta\theta}^{ki} = A_{13}^{ij}\sum_{m=1}^{n_\theta} W_{km}^1 U_{mj} + (A_{11}^{ij} + B_{12}^{ji})U_{kj} + A_{11}^{ij}\sum_{m=1}^{n_\theta} W_{km}^1 V_{mj} - (A_{13}^{ij} - B_{13}^{ji})V_{kj} = 0, \tag{16}$$

where $k = 1$ at $\theta = 0$ and $k = n_\theta$ at $\theta = \theta_0$.

In order to implement the boundary conditions, the boundary and domain degrees of freedom should be separated. Here, the vectors **b** and **d** are, respectively, used to represent the boundary and domain degrees of freedom, which are defined as

$$\mathbf{b} = [U_{11}, U_{12}, \ldots, U_{1n_n}, V_{n_\theta 1}, V_{n_\theta 2}, \ldots, V_{n_\theta n_r}]^{\mathrm{T}}, \quad \mathbf{d} = [U_{21}, U_{22}, \ldots, U_{n'_\theta n_n}, V_{21}, V_{22}., .., V_{n'_\theta n_r}]^{\mathrm{T}}, \tag{17}$$

where $n'_\theta = n_\theta - 1$. Using these definitions, the discretized form of the equations of motion and the boundary conditions can be written respectively, as

$$\mathbf{M}\ddot{\mathbf{d}} + \mathbf{K}_{dd}\mathbf{d} + \mathbf{K}_{db}\mathbf{b} = 0, \tag{18}$$

$$\mathbf{K}_{bb}\mathbf{b} + \mathbf{K}_{bd}\mathbf{d} = 0. \tag{19}$$

Based on the definitions of domain and boundary degrees of freedom given in Eq. (17), the elements of mass matrix $\mathbf{M}$, domain stiffness matrices $\mathbf{K}_{db}$ and $\mathbf{K}_{dd}$ are obtained from the discretized forms of the equations of motion. Also boundary stiffness matrices $\mathbf{K}_{bb}$ and $\mathbf{K}_{bd}$ are found using the discretized form of the boundary conditions in the same manner.

After eliminating the boundary degrees of freedom from Eq. (18) using Eq. (19), the result becomes

$$\mathbf{M}\ddot{\mathbf{d}} + \mathbf{K}\mathbf{d} = 0, \tag{20}$$

where $\mathbf{K} = \mathbf{K}_{dd} - \mathbf{K}_{db}\mathbf{K}_{bb}^{-1}\mathbf{K}_{bd}$.

In studying the free vibration analysis, one can assume that $\mathbf{d} = \mathbf{D}e^{i\omega t}$ in which ω is the natural frequency of the arch. Inserting this expression into Eq. (20), the final eigenvalue equation is obtained as

$$(-\omega^2\mathbf{M} + \mathbf{K})\mathbf{D} = 0. \tag{21}$$

Solving Eq. (21), the natural frequencies and mode shapes can be determined.

5. Results and discussion

In this section, first, the convergence behaviors of the method for evaluating the non-dimensional natural frequencies (ϖ_i) versus number of mathematical layers in the thickness direction and DQ grid points along the axial direction are verified. The antisymmetric cross-ply [0°/90°] laminates is chosen here, as these laminates suffer the worst stretching–bending coupling due to unsymmetrical lamination. In all the problems considered, the individual layers are taken to be of equal thickness and quadratic Lagrange interpolation functions are used through the thickness. The calculations are done for various values of the modular ratio E_1/E_2 and the other mechanical properties of each lamina are assumed to be $G_{12}/E_2 = G_{13}/E_2 = G_{23}/E_2 = 0.5$, $v_{12} = v_{13} = v_{23} = 0.25$.

In order to model the arch via the ABAQUS software, continuum plane stress elements with eight-node bilinear, hourglass control and reduced integration [22] are adopted to obtain accurate results. In each case, the convergence study was performed to obtain the converged results up to four significant digits and for brevity purpose, only the converged results are presented here. The number of elements to obtain the converged solutions depends on the type of boundary conditions and the value of thickness-to-length ratio; hence it differs from table to table.

As a first example, the convergence behaviors of the first three non-dimensional natural frequencies of the laminated arches for two different values of the thickness-to-length ratio and a large value of the orthotropy ratio are shown in Tables 1 and 2. The results are prepared for different numbers of the mathematical layers (n_m) of the layerwise theory. In addition to the ABAQUS results, the exact solutions of the first- and higher-order shear deformation theories [7,11] are also cited in these tables. For all cases, fast rates of convergence of the method are quite evident. It is found that two mathematical layers and nine grid points for DQM can yield results that are in close agreements with the other solutions. It is also obvious from the data presented in these tables that excellent agreement exists between the results of the present two-dimensional approach and those of the ABAQUS. Based on the data reported in these tables, the differences between the presented two-dimensional formulations and ABAQUS results and also HSDT are negligible. However, the results of the FSDT are greater than those of the other approaches. This is because the FSDT cannot simulate the transverse shear deformation accurately. Due to zig-zag nature of the displacement components in the layerwise theory, which enables the method to more accurately simulate the transverse shear deformation, it seems that the results of the present approach have better accuracy than those of the HSDT. It should be noted here that, better accuracy of DQ method with respect to finite element method was demonstrated in

Table 1
Convergence of the first three non-dimensional natural frequencies of the laminated cross-ply [0°/90°] simply supported curved beams ($\theta_0 = 57.296°$, $L/h = 10$, $E_1/E_2 = 40$)

n_x	$n_m = 2$			$n_m = 8$			$n_m = 16$		
	ϖ_1	ϖ_2	ϖ_3	ϖ_1	ϖ_2	ϖ_3	ϖ_1	ϖ_2	ϖ_3
7	3.0759	11.3812	21.7805	3.0474	11.1258	21.2111	3.0471	11.1244	21.2076
9	3.0248	11.4172	21.8435	2.9960	11.1623	21.2482	2.9957	11.1609	21.2445
13	3.0254	11.4137	21.6649	2.9966	11.1587	21.0695	2.9964	11.1573	21.0658
17	3.0254	11.4137	21.6644	2.9966	11.1587	21.0689	2.9964	11.1573	21.0652
23	3.0254	11.4137	21.6644	2.9966	11.1587	21.0689	2.9964	11.1573	21.0652
ABAQUS[a]							2.9909	11.1264	20.9926
HSDT [11]							3.0107	11.2043	21.1321
FSDT [7]							3.0814	11.9637	23.1804

[a] $n_e = 616$.

Table 2
Convergence of the first three non-dimensional natural frequencies of the laminated cross-ply [0°/90°] simply supported curved beams ($\theta_0 = 57.296°$, $L/h = 5$, $E_1/E_2 = 40$)

n_x	$n_m = 2$			$n_m = 8$			$n_m = 16$		
	ϖ_1	ϖ_2	ϖ_3	ϖ_1	ϖ_2	ϖ_3	ϖ_1	ϖ_2	ϖ_3
7	2.4774	7.7536	13.3881	2.4245	7.5527	13.1348	2.4243	7.5510	13.1300
9	2.4618	7.7602	13.5249	2.4086	7.5604	13.2624	2.4085	7.5587	13.2574
13	2.4620	7.7592	13.4515	2.4088	7.5594	13.1874	2.4087	7.5576	13.1824
17	2.4620	7.7592	13.4513	2.4088	7.5593	13.1872	2.4087	7.5576	13.1822
23	2.4620	7.7592	13.4513	2.4088	7.5593	13.1872	2.4087	7.5576	13.1822
ABAQUS[a]							2.4024	7.5312	13.1363
HSDT [11]							2.4208	7.5603	13.1246
FSDT [7]							2.5935	8.3979	14.466

[a] $n_e = 500$.

Table 3
Comparison of the first four non-dimensional natural frequencies of the laminated cross-ply [0°/90°] simply supported curved beams ($L/h = 10$)

	θ_0 (deg)	$E_1/E_2 = 15$				$E_1/E_2 = 40$			
		ϖ_1	ϖ_2	ϖ_3	ϖ_4	ϖ_1	ϖ_2	ϖ_3	ϖ_4
Present	90	2.8808	14.0479	29.3597	46.6904	2.3034	10.3571	20.2680	30.8938
ABAQUS[a]		2.8709	13.9904	29.2246	46.4634	2.2983	10.3252	20.1943	30.7759
Present	180	10.0822	25.1744	42.6101	61.2040	7.3459	17.2762	28.1096	39.4093
ABAQUS[b]		10.0236	25.0280	42.3681	60.8715	7.3165	17.2021	27.9876	39.2445
Present	270	2.8982	5.1885	19.7436	37.2694	2.2174	3.7257	13.4435	24.4849
ABAQUS[c]		2.8771	5.1514	19.6102	37.0324	2.2070	3.7077	13.3780	24.3677

[a] $n_e = 640$.
[b] $n_e = 1050$.
[c] $n_e = 1428$.

previous studies [16,17,21]. Since both the presented approach and ABAQUS model used in this study are based on the two-dimensional elasticity theory, the authors believe that the method proposed here yields more accurate results than the results generated using ABAQUS.

The results for the thick laminated deep arches with some combinations of classical boundary conditions are not yet available in the open literature. Hence, here some new results for these cases are presented in Tables 3–10. Comparisons between the results of the present method and those of the ABAQUS are made for different values of opening angles and two different values of thickness-to-length and orthotropy ratios.

Tables 3 and 4 give the first four natural frequency parameters for laminated cross ply simply supported arches for $L/h = 10$ and 5, respectively. Results for some other sets of boundary conditions are given in Tables 5–10. While it is difficult to draw general conclusions on the nature of variation of the natural frequency with opening angle it may be noted that for any given angle, the non-dimensional natural frequency parameters are higher for $L/h = 10$ than for $L/h = 5$. However, it should be mentioned that the actual natural frequencies will be lower for the more slender arch.

Also, it can be noted that the higher-order frequencies for arches with clamped, simply supported and clamped–simply supported edges, as one would expect in most cases, are less sensitive to boundary conditions. Although for brevity purposes the results for only two values of orthotropy ratios are presented here, however, based on the numerical experiment done during this work, it is found that increasing the orthotropy ratio resulted in a decrease in the non-dimensional frequencies.

In all cases, the maximum percentage error between the results of the present method and those of the ABAQUS software is less than 1% which shows the validity of the presented approach.

Table 4
Comparison of the first four non-dimensional natural frequencies of the laminated cross-ply [0°/90°] simply supported curved beams ($L/h = 5$)

	θ_0 (deg)	$E_1/E_2 = 15$				$E_1/E_2 = 40$			
		ϖ_1	ϖ_2	ϖ_3	ϖ_4	ϖ_1	ϖ_2	ϖ_3	ϖ_4
Present	90	2.5206	10.6525	20.1058	29.9594	1.8365	7.0274	12.7568	18.7268
ABAQUS[a]		2.5059	10.5920	20.0032	29.8274	1.8291	6.9969	12.7058	18.6617
Present	180	7.7364	17.6234	28.0531	38.5798	5.0577	11.1520	17.5292	23.9850
ABAQUS[b]		7.6840	17.5157	27.8955	38.3934	5.0319	11.0961	17.4395	23.8664
Present	270	2.4758	4.0615	14.2913	25.4291	1.6989	2.6265	9.0092	15.8761
ABAQUS[c]		2.4722	4.0398	14.1941	25.2683	1.6972	2.6161	8.9569	15.7769

[a] $n_e = 1008$.
[b] $n_e = 1280$.
[c] $n_e = 1710$.

Table 5
Comparison of the first four non-dimensional natural frequencies of the laminated cross-ply [0°/90°] clamped curved beams ($L/h = 10$)

	θ_0 (deg)	$E_1/E_2 = 15$				$E_1/E_2 = 40$			
		ϖ_1	ϖ_2	ϖ_3	ϖ_4	ϖ_1	ϖ_2	ϖ_3	ϖ_4
Present	90	18.5885	26.9657	41.8114	49.5849	12.6777	19.7844	32.3570	34.9780
ABAQUS[a]		18.5132	26.9556	41.8425	49.3914	12.6369	19.7504	32.2505	35.1869
Present	180	14.2157	26.3622	44.4845	57.9069	9.6321	17.6432	29.0050	39.0100
ABAQUS[b]		14.1432	26.2636	44.3013	57.9182	9.5954	17.5909	28.9081	38.9331
Present	270	10.4272	22.0748	38.9472	55.8021	7.1103	14.4866	25.2521	36.0501
ABAQUS[c]		10.3640	21.9735	38.7833	55.6281	7.0786	14.4381	25.1694	35.9545

[a] $n_e = 640$.
[b] $n_e = 1050$.
[c] $n_e = 1428$.

Table 6
Comparison of the first four non-dimensional natural frequencies of the laminated cross-ply [0°/90°] clamped curved beams ($L/h = 5$)

	θ_0 (deg)	$E_1/E_2 = 15$				$E_1/E_2 = 40$			
		ϖ_1	ϖ_2	ϖ_3	ϖ_4	ϖ_1	ϖ_2	ϖ_3	ϖ_4
Present	90	12.2221	15.3166	23.8728	29.6015	7.7813	11.4893	17.9500	18.7704
ABAQUS[a]		12.1789	15.4061	23.9244	29.5450	7.7587	11.5392	18.3670	18.7301
Present	180	9.4975	16.4178	27.2032	32.0964	6.0127	10.6210	17.2125	22.3908
ABAQUS[b]		9.4701	16.4338	27.1973	32.6738	5.9993	10.6332	17.2020	22.6223
Present	270	7.2958	14.1324	24.3379	33.7605	4.6582	8.9302	15.3536	21.5111
ABAQUS[c]		7.2911	14.1456	24.4190	34.0310	4.6565	8.9490	15.4078	21.6798

[a] $n_e = 1008$.
[b] $n_e = 1280$.
[c] $n_e = 1710$.

6. Conclusion

Based on the two-dimensional theory of elasticity, an accurate solution is presented for the free vibration analysis of thick laminated deep circular arches with some combinations of classical boundary conditions (simply supported, clamped and free). The formulations are general in the sense that the effects of the

Table 7
Comparison of the first four non-dimensional natural frequencies of the laminated cross-ply [0°/90°] clamped–free curved beams ($L/h = 10$)

	θ_0 (deg)	$E_1/E_2 = 15$				$E_1/E_2 = 40$			
		ϖ_1	ϖ_2	ϖ_3	ϖ_4	ϖ_1	ϖ_2	ϖ_3	ϖ_4
Present	90	1.6985	7.0299	19.9456	34.8932	1.3927	5.2611	14.1800	23.9202
ABAQUS[a]		1.6916	7.0058	19.8661	34.7699	1.3895	5.2485	14.1383	23.8534
Present	180	1.9284	5.3083	16.0730	31.2102	1.5471	3.9121	11.3158	21.1374
ABAQUS[b]		1.9178	5.2796	15.9879	31.0609	1.5425	3.8980	11.2742	21.0651
Present	270	2.3962	4.6872	12.4248	26.8177	1.8673	3.4072	8.6428	18.0057
ABAQUS[c]		2.3799	4.6528	12.3475	26.6672	1.8599	3.3897	8.6058	17.9352

[a] $n_e = 640$.
[b] $n_e = 1050$.
[c] $n_e = 1428$.

Table 8
Comparison of the first four non-dimensional natural frequencies of the laminated cross-ply [0°/90°] clamped–free curved beams ($L/h = 5$)

	θ_0 (deg)	$E_1/E_2 = 15$				$E_1/E_2 = 40$			
		ϖ_1	ϖ_2	ϖ_3	ϖ_4	ϖ_1	ϖ_2	ϖ_3	ϖ_4
Present	90	1.5812	5.3324	13.8514	21.6928	1.2164	3.6163	9.1228	14.2996
ABAQUS[a]		1.5717	5.3087	13.7975	21.6941	1.2118	3.6059	9.0988	14.2841
Present	180	1.7525	4.0976	11.2771	20.4697	1.2949	2.7211	7.3690	13.0761
ABAQUS[b]		1.7395	4.0738	11.2342	20.4071	1.2885	2.7104	7.3506	13.0474
Present	270	2.1030	3.6942	8.8569	18.1698	1.4867	2.4157	5.7248	11.5216
ABAQUS[c]		2.0992	3.6798	8.8498	18.1339	1.4841	2.4089	5.7261	11.5094

[a] $n_e = 1008$.
[b] $n_e = 1280$.
[c] $n_e = 1710$.

Table 9
Comparison of the first four non-dimensional natural frequencies of the laminated cross-ply [0°/90°] clamped–simply curved beams ($L/h = 10$)

	θ_0 (deg)	$E_1/E_2 = 15$				$E_1/E_2 = 40$			
		ϖ_1	ϖ_2	ϖ_3	ϖ_4	ϖ_1	ϖ_2	ϖ_3	ϖ_4
Present	90	4.4713	15.9007	30.7693	46.4623	3.3858	11.2700	20.9424	31.3285
ABAQUS[a]		4.4544	15.8367	30.6450	46.3398	3.3769	11.2346	20.8723	31.2233
Present	180	2.3805	11.7430	26.3544	43.1214	1.8351	8.2168	17.7692	28.3793
ABAQUS[b]		2.3678	11.6797	26.2234	42.9245	1.8293	8.1850	17.7028	28.2749
Present	270	2.4882	7.7015	21.2140	37.9661	1.9454	5.3431	14.1522	24.7843
ABAQUS[c]		2.4710	7.6504	21.0942	37.7696	1.9374	5.3178	14.0937	24.6862

[a] $n_e = 640$.
[b] $n_e = 1050$.
[c] $n_e = 1428$.

variation of arch curvature across the cross section, the transverse shear and normal stresses and inertias are included. Fast rates of convergence of the method are demonstrated and its high accuracy with low computational efforts are exhibited by comparing the results with existing solutions in the literature and also with those obtained using the ABAQUS software. For some different values of the geometrical and material

Table 10
Comparison of the first four non-dimensional natural frequencies of the laminated cross-ply [0°/90°] clamped–simply curved beams ($L/h=5$)

	θ_0 (deg)	$E_1/E_2=15$				$E_1/E_2=40$			
		ϖ_1	ϖ_2	ϖ_3	ϖ_4	ϖ_1	ϖ_2	ϖ_3	ϖ_4
Present	90	3.5539	11.1211	19.7928	26.2799	2.4080	7.2512	12.7855	18.4479
ABAQUS[a]		3.5357	11.0753	19.7454	26.4934	2.3988	7.2266	12.7497	18.4328
Present	180	2.0226	8.2987	17.4247	27.1464	1.4234	5.3439	11.0824	17.2277
ABAQUS[b]		2.0090	8.2645	17.3709	27.1186	1.4164	5.3276	11.0539	17.1952
Present	270	2.1867	5.5946	14.3822	24.7214	1.5519	3.5795	9.0733	15.5403
ABAQUS[c]		2.1848	5.5801	14.3481	24.6908	1.5505	3.5735	9.0595	15.5239

[a] $n_e=1008$.
[b] $n_e=1280$.
[c] $n_e=1710$.

properties such as opening angle, thickness-to-length and orthotropy ratios, the natural frequencies of the thick laminated arches with different set of boundary conditions are obtained. The solutions can be used as benchmarks for other numerical methods and also to evaluate the accuracy of the classical theories such as the first-order shear deformation theory.

Appendix A. DQ weighting coefficients

The basic idea of the differential quadrature method is that the derivative of a function, with respect to a space variable at a given sampling point is approximated as a weighted linear sum of the sampling points in the domain of that variable. In order to illustrate the DQ approximation, consider a function $f(x)$ having its field on a rectangular domain $0\leqslant x\leqslant L$. Let, in the given domain, the function values be known or desired on a grid of sampling points. According to DQ method, the rth derivative of a function $f(x)$ can be approximated as [16]

$$\left.\frac{\partial^r f(x)}{\partial x^r}\right|_{x=x_i}=\sum_{m=1}^{N_x} W^r_{im} f(x_m)=\sum_{m=1}^{N_x} W^r_{im} f_m \quad \text{for} \quad i=1,2,\ldots,N_x \quad \text{and} \quad r=1,2,\ldots,N_x-1. \tag{A.1}$$

From this equation one can deduce that the important components of DQ approximations are weighting coefficients and the choice of sampling points. In order to determine the weighting coefficients a set of test functions should be used in Eq. (A.1). For polynomial basis functions DQ, a set of Lagrange polynomials are employed as the test functions. The weighting coefficients for the first-order derivatives in x-direction are thus determined as [16]

$$W^1_{ij}=\begin{cases}\dfrac{1}{L(x_i-x_j)}\dfrac{M(x_i)}{M(x_j)} & \text{for } i\neq j,\\[2ex] & \qquad i,j=1,2\ldots,N_x,\\ -\sum\limits_{\substack{j=1\\ i\neq j}}^{N_x} W^1_{ij} & \text{for } i=j,\end{cases} \tag{A.2}$$

where

$$M(x_i)=\prod_{j=1,i\neq j}^{N_x}(x_i-x_j).$$

The weighting coefficients of second-order derivative can be obtained as

$$[W^2_{ij}]=[W^1_{ij}][W^1_{ij}]=[W^1_{ij}]^2. \tag{A.3}$$

In numerical computations, Chebyshev–Gauss–Lobatto quadrature points are used, that is

$$\frac{x_i}{L} = \frac{1}{2}\left\{1 - \cos\left[\frac{(i-1)\pi}{(N_x-1)}\right]\right\} \qquad \text{for} \quad i = 1, 2, \ldots, N_x. \tag{A.4}$$

Appendix B

In the present work the global quadratic shape functions are used through the thickness of the laminated arches, which can be expressed as

$$\varphi_i(r) = \begin{cases} 0, & r \leqslant r_{i-1}, r_{i+1} \leqslant r, \\ \dfrac{r^2 - (r_{i-1} + r_{i+1})r + r_{i-1}r_{i+1}}{r_i^2 - (r_{i-1} + r_{i+1})r_i + r_{i-1}r_{i+1}}, & r_{i-1} \leqslant r \leqslant r_{i+1}, \end{cases} \qquad i = 2, 4, \ldots, n_r - 1, \tag{B.1}$$

$$\varphi_i(r) = \begin{cases} 0, & R_i \leqslant r \leqslant r_{i-2}(i \neq 1), r_{i+2} \leqslant r \leqslant R_o(i \neq n_r), \\ \dfrac{r^2 - (r_{i-2} + r_{i-1})r + r_{i-2}r_{i-1}}{r_i^2 - (r_{i-2} + r_{i-1})r_i + r_{i-2}r_{i-1}}, & r_{i-2} \leqslant r \leqslant r_i(i \neq 1), \\ \dfrac{r^2 - (r_{i+1} + r_{i+2})r + r_{i+1}r_{i+2}}{r_i^2 - (r_{i+1} + r_{i+2})r_i + r_{i+1}r_{i+2}}, & r_i \leqslant r \leqslant r_{i+2}(i \neq n_r), \end{cases} \qquad i = 1, 3, \ldots, n_r, \tag{B.2}$$

where r_i is the radial position of the node i. Using Eqs. (B.1) and (B.2), one can obtain the stiffness coefficient appeared in the governing equations and the boundary conditions. The values of the stiffness coefficient depend on the location of the nodes i and j.

If i is an even number, then for $j = 1,2,\ldots, n_r$:

$$A_{mn}^{ij} = bC_{mn}^{(i/2)}\hat{A}_{ij}, \; B_{mn}^{ij} = bC_{mn}^{(i/2)}\hat{B}_{ij}, \; D_{mn}^{ij} = bC_{mn}^{(i/2)}\hat{D}_{ij}, \tag{B.3}$$

where

$$\begin{aligned} \hat{A}_{ij} = {} & \frac{\alpha_1\beta_1}{4}(R_3^4 - R_1^4) + \frac{(\alpha_1\beta_2 + \alpha_2\beta_1)}{3}(R_3^3 - R_1^3) + \frac{(\alpha_1\beta_3 + \alpha_3\beta_1 + \alpha_2\beta_2)}{2}(R_3^2 - R_1^2) \\ & + (\alpha_2\beta_3 + \alpha_3\beta_2)(R_3 - R_1) + \alpha_3\beta_3 \log(R_3/R_1), \\ \hat{B}_{ij} = {} & \frac{\alpha_1\beta_1}{2}(R_3^4 - R_1^4) + \frac{(\alpha_1\beta_2 + \alpha_2\beta_1)}{2}(R_3^3 - R_1^3) + \frac{(\alpha_1\beta_3 + \alpha_3\beta_1 + \alpha_2\beta_2)}{2}(R_3^2 - R_1^2) \\ & + \frac{(\alpha_2\beta_3 + \alpha_3\beta_2)}{2}(R_3 - R_1), \end{aligned}$$

$$\hat{D}_{ij} = \alpha_1\beta_1(R_3^4 - R_1^4) + \frac{(2\alpha_1\beta_2 + 2\alpha_2\beta_1)}{3}(R_3^3 - R_1^3) + \frac{\alpha_2\beta_2}{2}(R_3^2 - R_1^2), \tag{B.4}$$

and

$$\{\alpha_i\} = \hat{\mathbf{R}}^{-1}\mathbf{f}_\alpha, \quad \{\beta_i\} = \hat{\mathbf{R}}^{-1}\mathbf{f}_\beta, \tag{B.5}$$

with

$$\hat{\mathbf{R}} = \begin{bmatrix} R_1^2 & R_1 & 1 \\ R_2^2 & R_2 & 1 \\ R_3^2 & R_3 & 1 \end{bmatrix} \quad \text{and} \quad R_1 = r_{i-1}, \quad R_2 = r_i, \quad R_3 = r_{i+1}.$$

Also, $C_{mn}^{(i)}$ represent the elements of material stiffness coefficients of lamina i.

The elements of the vectors $\mathbf{f}_\alpha$ and $\mathbf{f}_\beta$ depend on the nodal numbers i and j,

$$\mathbf{f}_\alpha = \begin{bmatrix} 0, & 1, & 0 \end{bmatrix}^{\mathrm{T}} \quad \text{and} \quad \mathbf{f}_\beta = \begin{cases} \begin{bmatrix} 1, & 0, & 0 \end{bmatrix}^{\mathrm{T}} & \text{if } j = i-1, \\ \begin{bmatrix} 0, & 0, & 1 \end{bmatrix}^{\mathrm{T}} & \text{if } j = i+1. \end{cases} \tag{B.6}$$

If i is an odd number ($i = 1,3,\ldots, n_r-1$), then defining $i_R = (i-1)/2+1$ and $i_L = i_R - 1$, one has

$$\text{If } i=j=1: \quad A^{ij}_{mn} = bC^{(i)}_{mn}\hat{A}_{ij}, \quad B^{ij}_{mn} = bC^{(i)}_{mn}\hat{B}_{ij}, \quad D^{ij}_{mn} = bC^{(i)}_{mn}\hat{D}_{ij},$$
$$\text{with} \quad \mathbf{f}_\alpha = \mathbf{f}_\beta = \begin{bmatrix} 1, & 0, & 0 \end{bmatrix}^{\mathrm{T}} \quad \text{and} \quad R_1 = r_i, \quad R_2 = r_{i+1}, \quad R_3 = r_{i+2}. \tag{B.7}$$

$$\text{If } i=j=: n_r \quad A^{ij}_{mn} = bC^{(i_L)}_{mn}\hat{A}_{ij}, \quad B^{ij}_{mn} = bC^{(i_L)}_{mn}\hat{B}_{ij}, \quad D^{ij}_{mn} = bC^{(i_L)}_{mn}\hat{D}_{ij},$$
$$\text{with} \quad \mathbf{f}_\alpha = \mathbf{f}_\beta = \begin{bmatrix} 0, & 0, & 1 \end{bmatrix}^{\mathrm{T}} \quad \text{and} \quad R_1 = r_{i-2}, \quad R_2 = r_{i-1}, \quad R_3 = r_i. \tag{B.8}$$

If $i = j,\ i \neq 1$ and $i \neq n_r$:

$$\begin{aligned}
&A^{ij}_{mn} = b(C^{(i_L)}_{mn}\hat{A}^L_{ij} + C^{(i_R)}_{mn}\hat{A}^R_{ij}), \quad B^{ij}_{mn} = b(C^{(i_L)}_{mn}\hat{B}^L_{ij} + C^{(i_R)}_{mn}\hat{B}^R_{ij}), \\
&D^{ij}_{mn} = b(C^{(i_L)}_{mn}\hat{D}^L_{ij} + C^{(i_R)}_{mn}\hat{D}^R_{ij}), \quad \text{with} \quad \mathbf{f}_\alpha = \mathbf{f}_\beta = \begin{bmatrix} 0, & 0, & 1 \end{bmatrix}^{\mathrm{T}}, \\
&R_1 = r_i, \quad R_2 = r_{i+1}, \quad R_3 = r_{i+2} \quad \text{for} \quad (\,)^L_{ij}; \quad \text{and} \quad \mathbf{f}_\alpha = \mathbf{f}_\beta = \begin{bmatrix} 1, & 0, & 0 \end{bmatrix}^{\mathrm{T}}, \\
&R_1 = r_{i-2}, \quad R_2 = r_{i-1}, \quad R_3 = r_i \quad \text{for} \quad (\,)^R_{ij}.
\end{aligned} \tag{B.9}$$

$$\text{If } j = i-1: \quad A^{ij}_{mn} = bC^{(i_L)}_{mn}\hat{A}_{ij}, \quad B^{ij}_{mn} = bC^{(i_L)}_{mn}\hat{B}_{ij}, \quad D^{ij}_{mn} = bC^{(i_L)}_{mn}\hat{D}_{ij}, \quad \text{with} \quad \mathbf{f}_\alpha = \begin{bmatrix} 0, & 0, & 1 \end{bmatrix}^{\mathrm{T}},$$
$$f_\beta = \begin{bmatrix} 0, & 1, & 0 \end{bmatrix}^{\mathrm{T}} \quad \text{and} \quad R_1 = r_{i-2}, \quad R_2 = r_{i-1}, \quad R_3 = r_i. \tag{B.10}$$

$$\text{If } j = i+1: \quad A^{ij}_{mn} = bC^{(i_R)}_{mn}\hat{A}_{ij}, \quad B^{ij}_{mn} = bC^{(i_R)}_{mn}\hat{B}_{ij}, \quad D^{ij}_{mn} = bC^{(i_R)}_{mn}\hat{D}_{ij}, \quad \text{with} \quad \mathbf{f}_\alpha = \begin{bmatrix} 1, & 0, & 0 \end{bmatrix}^{\mathrm{T}},$$
$$\mathbf{f}_\beta = \begin{bmatrix} 0, & 1, & 0 \end{bmatrix}^{\mathrm{T}} \quad \text{and} \quad R_1 = r_i, R_2 = r_{i+1}, R_3 = r_{i+2}. \tag{B.11}$$

$$\text{If } j = i+2: \quad A^{ij}_{mn} = bC^{(i_R)}_{mn}\hat{A}_{ij}, \quad B^{ij}_{mn} = bC^{(i_R)}_{mn}\hat{B}_{ij}, \quad D^{ij}_{mn} = bC^{(i_R)}_{mn}\hat{D}_{ij}, \quad \text{with} \quad \mathbf{f}_\alpha = \begin{bmatrix} 1, & 0, & 0 \end{bmatrix}^{\mathrm{T}},$$
$$\mathbf{f}_\beta = \begin{bmatrix} 0, & 0, & 1 \end{bmatrix}^{\mathrm{T}} \quad \text{and} \quad R_1 = r_i, \quad R_2 = r_{i+1}, \quad R_3 = r_{i+2}. \tag{B.12}$$

$$\text{If } j = i-2: \quad A^{ij}_{mn} = bC^{(i_L)}_{mn}\hat{A}_{ij}, B^{ij}_{mn} = bC^{(i_L)}_{mn}\hat{B}_{ij}, D^{ij}_{mn} = bC^{(i_L)}_{mn}\hat{D}_{ij}, \text{ with } \mathbf{f}_\alpha = \begin{bmatrix} 0, & 0, & 1 \end{bmatrix}^{\mathrm{T}},$$
$$\mathbf{f}_\beta = \begin{bmatrix} 1, & 0, & 0 \end{bmatrix}^{\mathrm{T}} \text{ and } R_1 = r_{i-2}, R_2 = r_{i-1}, R_3 = r_i. \tag{B.13}$$

References

[1] P.P.A. Laura, M.J. Maurizi, Recent research on vibrations of arch-type structures, *Shock and Vibration Digest* 19 (1987) 6–9.

[2] P. Childamparam, A.W. Leissa, Vibration of planer curved beams, rings, and arches, *Applied Mechanics Review* 46 (1993) 467–483.

[3] G. Karami, P. Malekzadeh, In-plane free vibration analysis of circular arches with varying cross sections, *Journal of Sound and Vibration* 274 (2004) 777–799.

[4] A. Bhimaraddi, A.J. Carr, P.J. Moss, Generalized finite element analysis of laminated curved beams with constant curvature, *Computers and Structures* 31 (1989) 309–317.

[5] M.S. Qatu, In-plane vibration of slightly curved laminated composite beams, *Journal of Sound and Vibration* 159 (1993) 327–338.

[6] M.S. Qatu, A.A. Elsharkawy, Vibration of laminated composite arches with deep curvature and arbitrary boundaries, *Computers and Structures* 47 (1993) 305–311.

[7] M.S. Qatu, Theories and analysis of thin and moderately thick laminated composite curved beams, *International Journal of Solids and Structures* 30 (1993) 2743–2756.

[8] M.S. Qatu, *Vibration of Composite Shells and Plates*, Elsevier, Amsterdam, 2004, pp. 416.

[9] B.P. Patel, M. Ganapathi, J. Saravanan, Shear flexible field-consistent curved spline beam element for vibration analysis, *International Journal for Numerical Methods in Engineering* 46 (1999) 387–407.

[10] Y.P. Tseng, C.S. Huang, C.J. Lin, In-plane vibration of laminated curved beams with variable curvature by dynamic stiffness analysis, *Composite Structures* 50 (2000) 103–114.
[11] H. Matsunaga, Free vibration and stability of laminated composite circular arches subjected to initial axial stress, *Journal of Sound and Vibration* 271 (2004) 651–670.
[12] J.N. Reddy, A generalization of two-dimensional theories of laminated composite plates, *Communications in Applied Numerical Methods* 3 (1987) 173–180.
[13] J.N. Reddy, *Mechanics of Laminated Composite Plates Theory and Analysis*, CRC Press, Boca Raton, FL, 1997.
[14] A.R. Setoodeh, G. Karami, A solution for the vibration and buckling of composite laminates with elastically restrained edges, *Composite Structures* 60 (2003) 245–253.
[15] A.R. Setoodeh, G. Karami, Static, free vibration and buckling analysis of anisotropic thick laminated composite plates on distributed and point elastic supports using a 3-D layer-wise FEM, *Engineering Structures* 26 (2004) 211–220.
[16] C.W. Bert, M. Malik, Differential quadrature method in computational mechanics: a review, *Applied Mechanics Review* 49 (1996) 1–27.
[17] G. Karami, P. Malekzadeh, A new differential quadrature methodology for beam analysis and the associated DQEM, *Computer Methods in Applied Mechanics and Engineering* 191 (2002) 3509–3526.
[18] G. Karami, P. Malekzadeh, Application of a new differential quadrature methodology for free vibration analysis of plates, *International Journal for Numerical Methods in Engineering* 56 (2003) 847–867.
[19] P. Malekzadeh, A.R. Setoodeh, Large deformation analysis of moderately thick laminated plates on nonlinear elastic foundations by DQM, *Composite Structures* 80 (2007) 569–579.
[20] P. Malekzadeh, A.R. Fiouz, *Composite Structures* 80 (2007) 196–206.
[21] G. Karami, P. Malekzadeh, S.A. Shahpari, A DQEM for vibration of shear deformable nonuniform beams with general boundary conditions, *Engineering Structures* 25 (2003) 1169–1178.
[22] H.D. Hibbit, B.I. Karlsson, K. Sorensen, *ABAQUS Users and Theory Manuals, Version 6.2*, HKS Inc, RI, 1998.